JACS
JOURNAL OF THE AMERICAN CHEMICAL SOCIETY
Article
pubs.acs.org/JACS

Computational Study of Rh-Catalyzed Carboacylation of Olefins: Ligand-Promoted Rhodacycle Isomerization Enables Regioselective C−C Bond Functionalization of Benzocyclobutenones

Gang Lu,[†] Cheng Fang,[†] Tao Xu,[‡,§] Guangbin Dong,[‡] and Peng Liu*[,†]

[†]Department of Chemistry, University of Pittsburgh, Pittsburgh, Pennsylvania 15260, United States
[‡]Department of Chemistry, University of Texas at Austin, Austin, Texas 78712, United States
[§]School of Medicine and Pharmacy, Ocean University of China, Qingdao 266003, P. R. China

Supporting Information

ABSTRACT: The mechanism, reactivity, regio- and enantioselectivity of the Rh-catalyzed carboacylation of benzocyclobutenones are investigated using density functional theory (DFT) calculations. The calculations indicate that the selective activation of the relatively unreactive C1−C2 bond in benzocyclobutenone is achieved via initial C1−C8 bond oxidative addition, followed by rhodacycle isomerization via decarbonylation and CO insertion. Analysis of different ligand steric parameters, ligand steric contour maps, and the computed activation barriers revealed the origin of the positive correlation between ligand bite angle and reactivity. The increase of reactivity with bulkier ligands is attributed to the release of ligand−substrate repulsions in the P−Rh−P plane during the rate-determining CO insertion step. The enantioselectivity in reactions with the (*R*)-SEGPHOS ligand is controlled by the steric repulsion between the C8 methylene group in the substrate and the equatorial phenyl group on the chiral ligand in the olefin migratory insertion step.

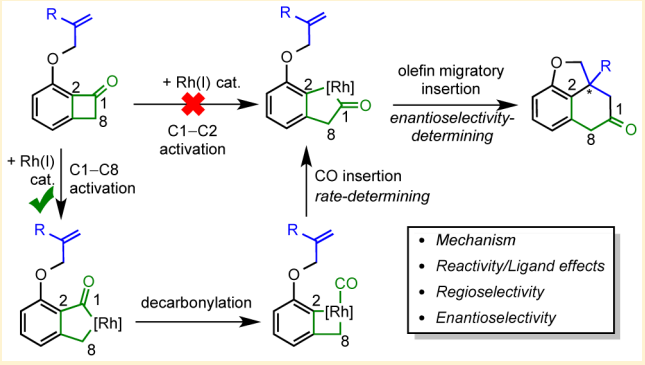

INTRODUCTION

Catalytic carbon−carbon bond activation and functionalization offer great potential for the synthesis of complex product scaffolds. A number of synthetically useful reactions featuring C−C bond cleavage and subsequent formation of one or more new C−C bonds have been recently developed and applied to a wide variety of substrates.[1] In particular, three- and four-membered carbocycles[2] are privileged substrates for synthesizing fused carbocycles, key motifs in various biologically important natural products. In this regard, the Dong group recently reported a series of transformations triggered by insertion of a rhodium catalyst into the relatively inert C1−C2 bond in benzocyclobutenones,[3] including carboacylation of olefins (Scheme 1),[4] decarbonylative spirocyclization,[5] and alkyne−benzocyclobutenone couplings.[6]

In contrast to the rapid experimental advances, no mechanistic or computational studies on these reactions have been reported.[7] Notwithstanding their inertness, carbon−carbon bonds may be cleaved via several different mechanisms in the presence of a transition-metal catalyst, including oxidative addition, *β*-carbon elimination, and retro-allylation.[8] Recent computational studies on C−C bond activation reactions focused on the cleavage of the polar C−CN bond[9] and the ring opening of strained vinylcyclopropanes,[10] cyclopropylidenes,[11] and cyclopropenones.[12−14] Computational studies from the Morokuma and Dang groups revealed that Rh-catalyzed ring opening of benzocyclobutenols and cyclobutanols takes place via deprotonation of the alcohol to form a Rh(I) alkoxide intermediate and subsequent *β*-carbon elimination (Scheme 2a).[15] However, the mechanism and the origin of the high level of regioselectivity in the Rh-catalyzed C−C bond activation with benzocyclobutenones are still not known. Based on the seminal organometallic studies by Liebeskind,[16] the originally proposed pathway (path b, Scheme

Scheme 1. Rh-Catalyzed Carboacylation of Olefins

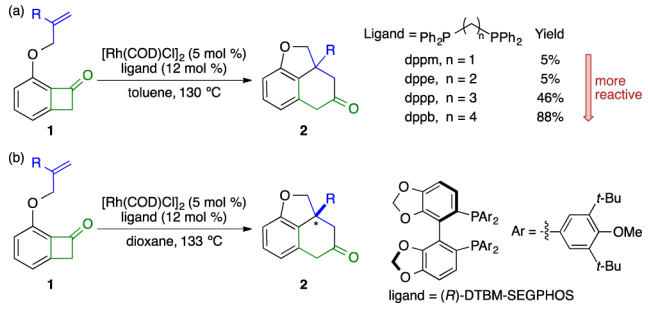

Received: May 5, 2015
Published: June 8, 2015

DOI: 10.1021/jacs.5b04691
J. Am. Chem. Soc. 2015, 137, 8274−8283

Scheme 2. Possible Mechanisms for Rh-Catalyzed C−C Bond Activation

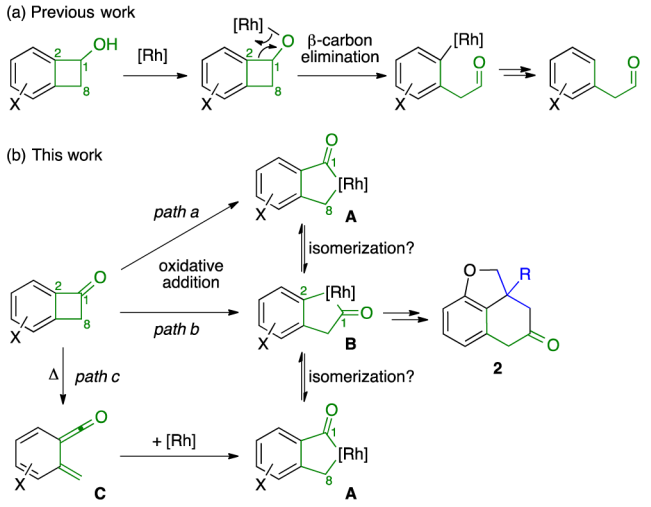

2b) involves the oxidative addition of the rhodium catalyst into the C1(sp^2)−C2(sp^2) bond to form a five-membered rhodacycle intermediate **B**, followed by olefin migratory insertion and reductive elimination to yield product **2**. On the other hand, oxidative addition may occur at the weaker C1(sp^2)−C8(sp^3) bond[3] in the substrate (path a). Although only the C1−C2 activation product **2** was observed, the C1−C8 oxidative addition intermediate **A** may undergo decarbonylation and CO insertion to isomerize to rhodacycle **B** prior to the subsequent new C−C bond formation steps. Additionally, other possible mechanisms, such as thermal electrocyclic ring-opening (path c), cannot be ruled out.[17]

Here we report the first computational study on the mechanism of the rhodium-catalyzed carboacylation of olefins with benzocyclobutenones. The calculations indicated a rhodacycle isomerization mechanism (path a, **A** → **B**) is responsible for the high regioselectivity for the C1−C2 bond activation, leaving the relatively weak C1−C8 bond intact.[18] The effects of ligands on the rate-determining rhodacycle isomerization step were analyzed using different ligand steric parameters, including ligand bite angle,[19] buried volume,[20] and steric contour map.[21] In addition, the origin of enantioselectivity in the asymmetric version of the reaction was investigated computationally (Scheme 1b).

COMPUTATIONAL METHODS

The B3LYP density functional and a mixed basis set of LANL2DZ for Rh and 6-31G(d) for other atoms were used in geometry optimizations. Single-point energies were calculated with M06 and a mixed basis set of SDD for Rh and 6-311+G(d,p) for other atoms. Solvation energy corrections were calculated using the SMD model. In accordance with the experimental conditions, toluene was used as solvent in the calculations for the reactions with dppm (1,1-bis(diphenylphosphino)methane, $Ph_2PCH_2PPh_2$), dppe (1,2-bis-(diphenylphosphino)ethane, $Ph_2P(CH_2)_2PPh_2$), dppp (1,3-bis-(diphenylphosphino)propane, $Ph_2P(CH_2)_3PPh_2$), and dppb (1,4-bis(diphenylphosphino)butane, and $Ph_2P(CH_2)_4PPh_2$) ligands, and dioxane was used as solvent in calculations with the (*R*)-SEGPHOS ligand. Calculations using M06 for geometry optimizations were also performed for the most favorable pathway. The results are consistent with those using B3LYP in geometry optimizations (see details in Supporting Information, Figure S1). All calculations were performed with Gaussian 09.[22] Ligand buried volume (V_{Bur}%) was calculated using the SambVca program[23] based on the B3LYP-optimized geometries.

RESULTS AND DISCUSSION

Oxidative Addition Reaction Pathways for the C−C Bond Cleavage. We first considered the possible mechanisms involving oxidative addition in the carbon−carbon bond activation step (Scheme 3). In path a, oxidative addition of

Scheme 3. Proposed Oxidative Addition Reaction Pathways

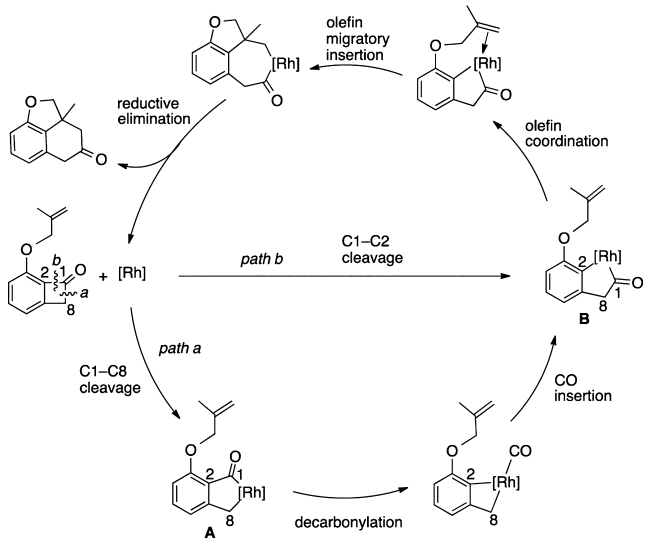

the C1(sp^2)−C8(sp^3) bond in benzocyclobutenone leads to a rhodacycle intermediate **A**, which then undergoes decarbonylation and CO insertion to the Rh−C8 bond to form intermediate **B**. In path b, oxidative addition of the C1(sp^2)−C2(sp^2) bond directly forms rhodacycle intermediate **B**. Complex **B** then undergoes olefin migratory insertion and reductive elimination to yield the tricyclic ketone product. We performed DFT calculations on both pathways of the reaction of benzocyclobutenone **1** (Scheme 1a, R = Me). The dppb ligand was used in the calculations as it was found to be the most effective ligand in experiment (Scheme 1a). The effects of ligands on reactivity and enantioselectivity will be discussed in details later.

The computed potential energy profiles for the possible pathways in the oxidative addition step are shown in Figure 1. All energies are with respect to the substrate **1** and the active catalyst, (dppb)RhCl. The active catalyst is expected to be generated from the dissociation of the dimeric catalyst precursor $[Rh(COD)Cl]_2$ followed by ligand substitution with the bidentate phosphine, dppb. Coordination of the rhodium to the carbonyl group in the reactant leads to an η^1-oxygen bound complex **3**, which is only 1.0 kcal/mol more stable than the separate catalyst and reactant. After a systematic conformational search for the oxidative addition transition states and the intermediates (see details in Figure S2), we located the most stable oxidative addition transition states **4-TS** and **6-TS** and rhodacycle intermediates **5** and **7** in the C1−C2 and C1−C8 bond cleavage pathways, respectively. The lowest energy conformers of intermediates **5** and **7** are both square-based pyramidal complexes with the acyl group (C1) at the apical position and the aryl (C2) or alkyl (C8) group, the Cl, and the dppb ligand in the equatorial plane (Figure 2). Isomers with an equatorial acyl group are at least 13.8 and 5.5 kcal/mol

DOI: 10.1021/jacs.5b04691
J. Am. Chem. Soc. 2015, 137, 8274−8283

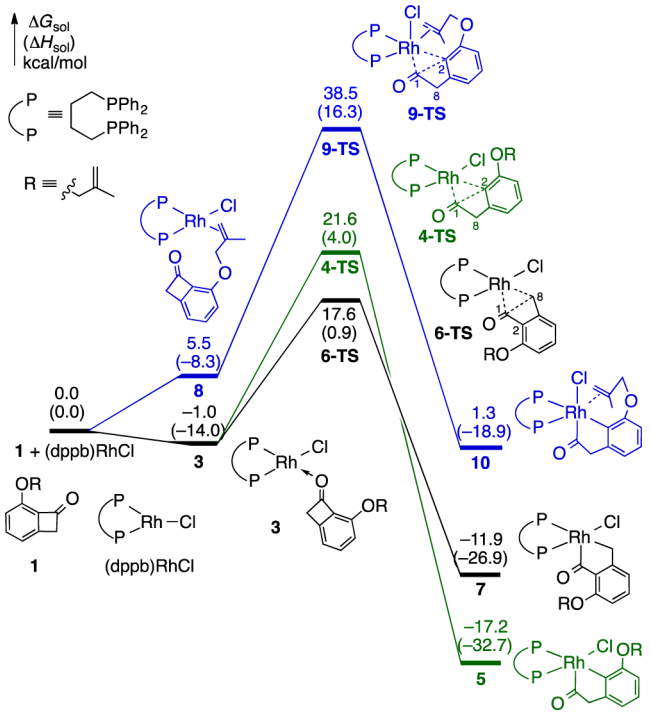

Figure 1. Energy profiles of the oxidative addition pathways. Black: the favored C1−C8 bond oxidative addition; blue: C1−C2 bond oxidative addition with olefin coordinated to Rh;[27] green: C1−C2 bond oxidative addition without olefin coordination.

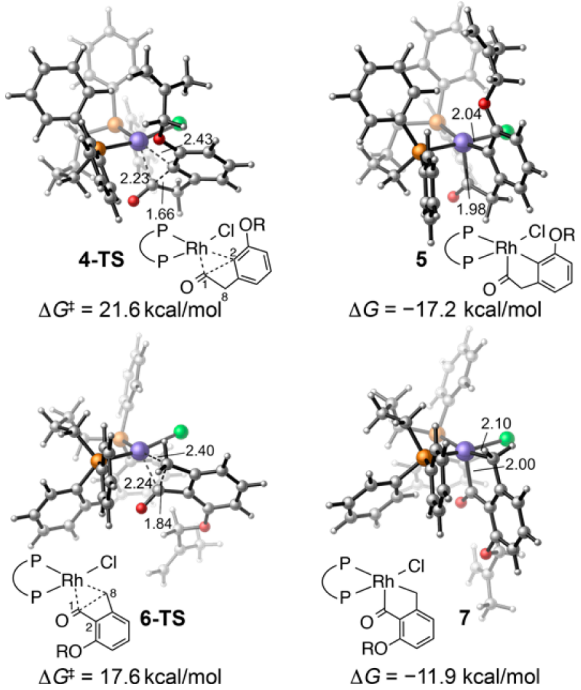

Figure 2. Optimized structures of the oxidative addition transition states and intermediates in the C1−C2 bond cleavage pathway (**4-TS** and **5**) and the C1−C8 bond cleavage pathway (**6-TS** and **7**).

less stable than **5** and **7**, respectively. The oxidative addition transition states **4-TS** and **6-TS** also adopt the apical-carbonyl geometry. The barrier of the C1−C2 oxidative addition (**4-TS**) is 4.0 kcal/mol higher than that of the C1−C8 oxidative addition (**6-TS**), indicating the relative reactivity is dependent upon the strengths of the C−C bond. The C1−C8 bond cleavage transition state **6-TS** is also favored sterically, as the bulky alkoxy group (OR) is placed further away from the ligand in **6-TS** than in **4-TS**. Both oxidative addition pathways are highly exergonic and irreversible (from **7** or **5**, the barriers for subsequent forward reaction steps are lower than the reverse barrier to regenerate **3**, see below for details). Thus, the selectivity in the initial oxidative addition step is kinetically controlled, leading to the C1−C8 oxidative addition intermediate **7** exclusively, although the rhodacycle intermediate **5** from the C1−C2 bond cleavage is 5.3 kcal/mol more stable than **7**.

There is an empty coordination site in the 16-electron square-based pyramidal complexes **5** and **7** and in the oxidative addition transition states **4-TS** and **6-TS**. We then investigated whether a π coordination between the alkenyl group on the substrate and the rhodium will facilitate the oxidative addition step. Similar olefin-directing effects have been proposed to promote hydroacylation,[24] C−H bond activation,[25] and C−C coupling reactions.[26] Here, the olefin coordination is geometrically impossible in the C1−C8 oxidative addition product **7** and the corresponding transition state **6-TS**, where the OR group is on the opposite face to the empty coordination site. In contrast, the olefin may coordinate to the metal in the C1−C2 oxidative addition (the blue pathway in Figure 1). The oxidative addition transition state with olefin coordination at the equatorial site (**9-TS**) was found to require a substantially higher barrier than **4-TS** and **6-TS**.[27] The transition state with olefin coordination at the apical site cannot be located. The unfavorable olefin coordination is due to the ring strain to form the chelated π complex and the steric repulsion between the olefin and the phosphine ligand in **9-TS**. Similarly, olefin coordination is also unfavorable in the oxidative addition intermediate (**10**) and the reactant complex (**8**). These results indicate that the C1−C2 selectivity in the carboacylation reaction is not a result of olefin directing effects.

Alternative C−C Bond Cleavage Mechanisms. Benzocyclobutenone derivatives are known to undergo electrocyclic ring opening at elevated temperature.[17] We computed the pathways of the thermal electrocyclic ring opening of benzocyclobutenone **1** (Figure 3). The ring opening of the

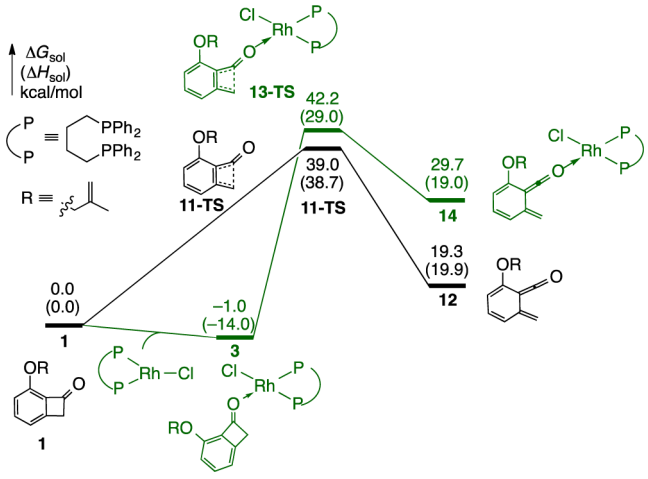

Figure 3. Energy profiles of the thermal electrocyclic ring opening pathways. Black: ring opening of benzocyclobutenone **1**; green: ring opening of the rhodium-bound complex **3**.

DOI: 10.1021/jacs.5b04691
J. Am. Chem. Soc. 2015, 137, 8274−8283

rhodium-bound complex **3** was also investigated to explore whether the ketone-Lewis acid coordination could promote the ring opening.[28] The thermal electrocyclic ring opening of benzocyclobutenone **1** requires a high barrier of 39.0 kcal/mol (**11-TS**) and is endergonic by 19.3 kcal/mol. Due to the loss of aromaticity, the benzocyclobutenone electrocyclic ring opening is much less favorable than the ring opening of cyclobutenones.[29] The ring opening of the rhodium-bound complex **3** is even less favorable (green pathway in Figure 3) in terms of activation free energies due to unfavorable entropic effects. Thus, the electrocyclic ring opening mechanisms are ruled out.

We next investigated a stepwise C−C bond cleavage mechanism, which involves nucleophilic addition to the ketone to form a zwitterionic alkoxide **15** followed by ring expansion to form the five-membered rhodacycle **5** or **7** (Scheme 4). The

Scheme 4. A Stepwise C−C Bond Cleavage Mechanism

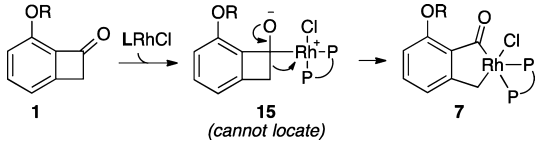

zwitterionic alkoxide cannot be located in the geometry optimization. Reaction coordinate scans suggested this pathway requires much higher barrier than the oxidative addition mechanism (see details in Figure S3). Overall, the above calculations revealed an oxidative addition mechanism for the C−C bond cleavage process, in which the two Rh−C bonds are forming simultaneously (see Figure S4 for intrinsic reaction coordinate calculations on the changes of Rh−C bond distances in the oxidative addition pathway).

Isomerization of the Rhodacycle Intermediate via Decarbonylation and CO Insertion. Since the oxidative addition of the C1−C8 bond of benzocyclobutenone **1** to form rhodacycle **7** is much more favorable kinetically, isomerization of **7** to **5** is necessary before olefin migratory insertion to yield the observed C1−C2 bond activation product **2**. One of the possible pathways for such isomerization is via reversible oxidative addition to form the thermodynamically more stable rhodacycle intermediate **5** (**7** → **6-TS** → **3** → **4-TS** → **5**). This process requires a barrier of 33.5 kcal/mol with respective to **7**. A more feasible isomerization pathway involves decarbonylation of **7**[30] that cleaves the C1−C2 bond followed by insertion of the CO ligand[31] into the Rh−C8 bond (Figure 4). As there is no empty coordination site *cis* to the acyl group in the square-based pyramidal complex **7**, the direct decarbonylation from **7** accompanies rearrangement of the equatorial alkyl group to the apical position, which requires a high barrier of 42.0 kcal/mol (**17′-TS**). A more favorable decarbonylation pathway takes place via ligand isomerization to form a square-based pyramidal complex **16** with a vacant binding site adjacent to the acyl group. Although **16** is 13.9 kcal/mol less stable than **7**, decarbonylation from **16** (**17-TS**, Figure 5) requires a much lower barrier than the direct decarbonylation from **7**. The decarbonylation leads to a highly strained benzorhodacyclobutene complex **18**, which is 20.5 kcal/mol less stable than **7**. In **18**, the CO ligand is *cis* to the benzylic carbon (C8). This geometry allows for the CO insertion into the Rh−C8 bond via **19-TS** (see Figure S5 for other less favorable isomers) to form the benzorhodacyclopentenone intermediate **20**, which then undergoes ligand isomerization to form the more stable isomer **5**. The barriers for decarbonylation (**17-TS**) and CO insertion (**19-TS**) are 24.2 and 28.1 kcal/mol with respect to **7**. This isomerization pathway requires a much lower barrier than the reversible oxidative addition to generate **5**.

We also computed two possible side-reaction pathways from the decarbonylation intermediate **18**. CO elimination from **18** forms five-coordinated intermediate **21**, which is 4.1 kcal/mol higher in energy than the CO insertion transition state **19-TS**. C−C reductive elimination from **18** to form benzocyclopropene **24** also requires much higher barrier than CO insertion.

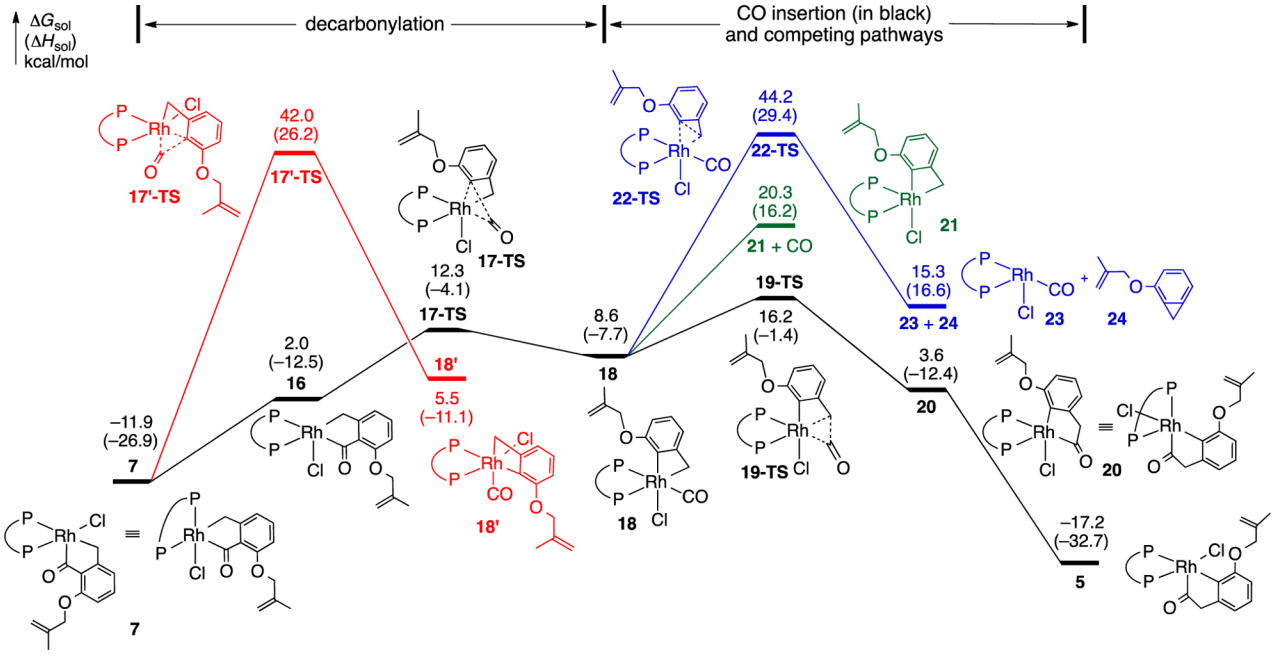

Figure 4. Energy profiles of the decarbonylation and CO insertion steps. Black: the preferred pathway; red: the unfavorable direct decarbonylation from **7**; blue: the side reaction to form benzocyclopropene **24**; green: the side reaction of CO elimination from **18**.

DOI: 10.1021/jacs.5b04691
J. Am. Chem. Soc. 2015, 137, 8274−8283

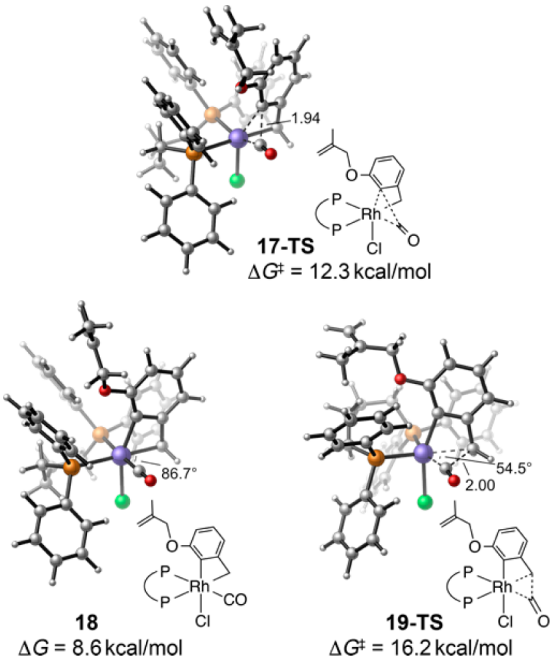

Figure 5. Optimized geometries of the decarbonylation transition state (**17-TS**), the octahedral intermediate (**18**), and the CO insertion transition state (**19-TS**).

Although similar CO elimination products and benzocyclopropene derivatives are observed in related systems,[30a,b,32] these pathways are both less favorable than CO insertion (**19-TS**), which has a barrier of only 7.6 kcal/mol with respect to **18**.

Olefin Migratory Insertion and Reductive Elimination. After the formation of **5**, two olefin migratory insertion pathways are possible. Olefin insertion at the position trans to the acyl group (**25′-TS**) requires prohibitively high energy ($\Delta G^{\ddagger}_{(5-25'\text{-TS})}$ = 48.2 kcal/mol). Instead, olefin coordination *cis* to the acyl group leads to π complex **10**, which allows the olefin attack to be perpendicular to the five-membered rhodacycle. This olefin migratory insertion pathway requires a barrier of 23.3 kcal/mol (**25-TS**, Figure 7, see Figure S6 for other less favorable isomers). This is much more facile than the trans attack (**25′-TS**) and is faster than the preceding rhodacycle isomerization step, which requires a barrier of 28.1 kcal/mol. It is expected the migratory insertion of sterically hindered internal olefin would require a much higher barrier. In addition, olefin migratory insertion of substrate **1a** with one more methylene group on the tether to form a six-membered dihydropyran ring also requires significantly higher barrier than the insertion to form the five-membered dihydrofuran product **2**.[33] This indicates in reactions with bulky olefins and with longer tethers that the olefin migratory insertion may become rate-determining.[7b]

Finally, C−C reductive elimination from the seven-membered rhodacycle intermediate **26** proceeds with a relatively low barrier of 19.7 kcal/mol (**27-TS**) with respect to **5** to form the product **2** and regenerates the active catalyst (dppb)RhCl.

In summary, the catalytic cycle of the Rh-catalyzed carboacylation of benzocyclobutenone **1** proceeds via oxidative addition of the C1−C8 bond, rhodacycle isomerization via decarbonylation and CO insertion, olefin migratory insertion, and reductive elimination (path a, Scheme 3). The computed energy profile of the complete catalytic cycle is shown in the black pathways in Figures 1, 4, and 6. The rate-determining step in the overall reaction is the CO insertion (**19-TS**), with a barrier of 28.1 kcal/mol with respect to the resting state **7**. The irreversible olefin migratory insertion (**25-TS**) is the enantioselectivity-determining step in the asymmetric variant of this reaction with chiral ligands, such as SEGPHOS. The effects of ligands on reactivity and enantioselectivity are discussed in the following sections.

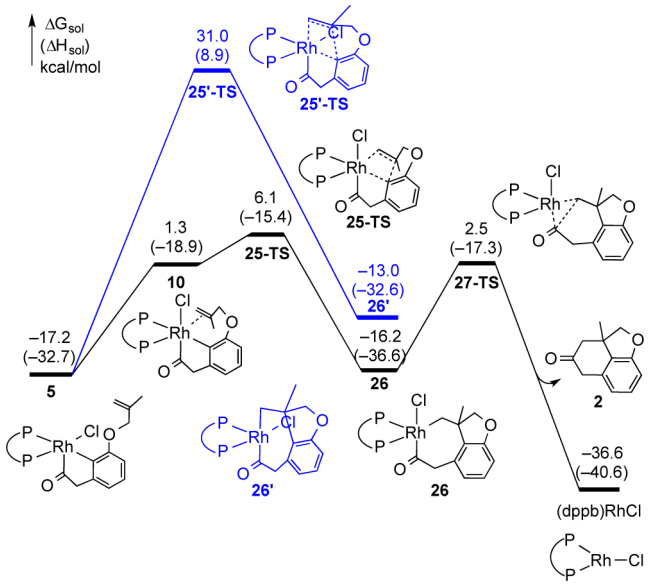

Figure 6. Energy profiles of the olefin insertion and reductive elimination steps.

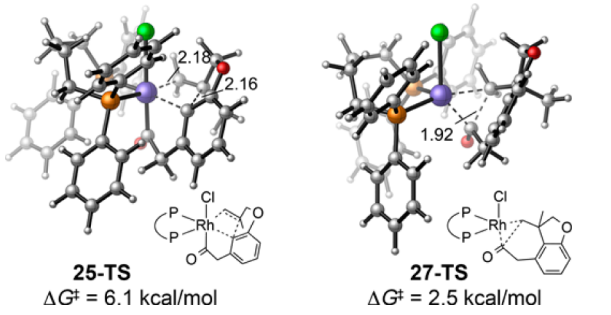

Figure 7. Optimized geometries of the olefin insertion (**25-TS**) and reductive elimination (**27-TS**) transition states.

Effects of Ligand on Reactivity. The reactivity of the rhodium catalyst in the carboacylation reaction is greatly affected by the ligand (Scheme 1a). Experimental studies with a series of bidentate phosphine ligands indicated a positive correlation between the bite angle of the ligands and the yield.[4a] However, it was not clear why bulkier bidentate ligands promote the carboacylation reaction. At first glance, the experimental trend does not appear to agree with the computed mechanism: If the rate of the reaction is determined by the energy difference between the five-coordinated resting state rhodacycle **7** and the more crowded six-coordinated CO insertion transition state **19-TS**, then why would bulkier ligands lead to faster reaction?

To analyze the origins of ligand steric effects on reactivity, we computed the activation barriers of the rate-determining CO

DOI: 10.1021/jacs.5b04691
J. Am. Chem. Soc. 2015, 137, 8274−8283

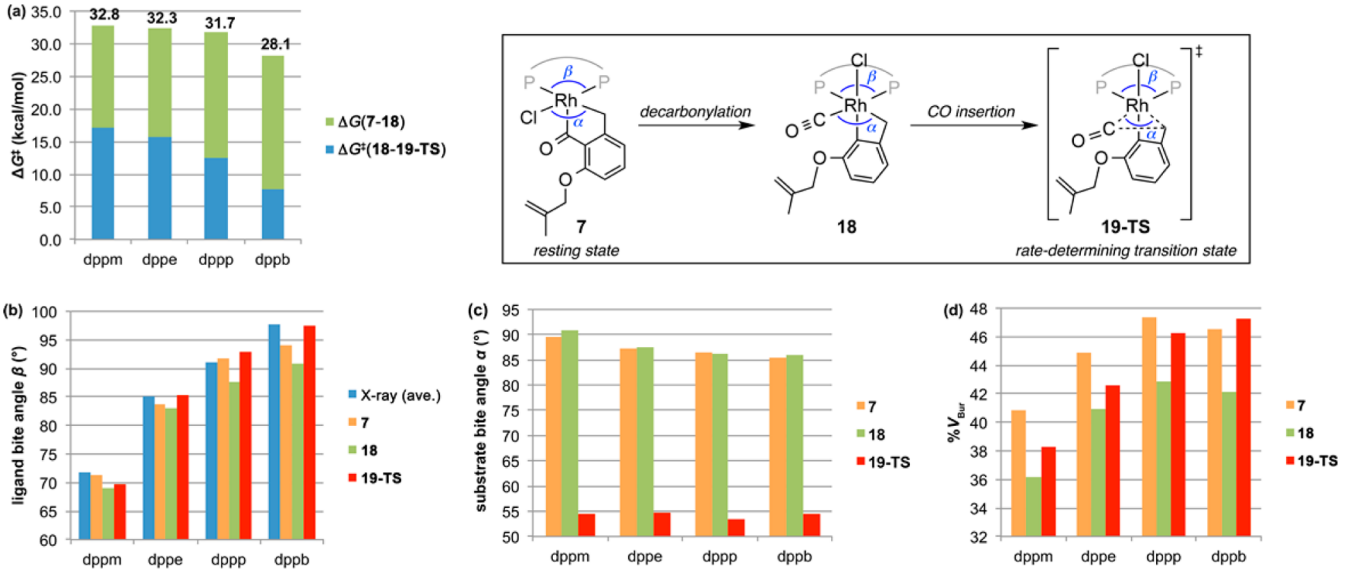

Figure 8. (a) Ligands effects on activation barrier. The overall barrier is dissected to the energy difference between **7** and **18** (ΔG(**7**-**18**), shown in green bars) and between **18** and **19-TS** ($\Delta G^{\ddagger}$(**18**-**19-TS**), shown in blue bars). (b) Ligand bite angles (β) reported in the literature[19a] (average bite angles in X-ray structures) and the computed bite angles in complexes **7**, **18**, and **19-TS**. (c) Substrate bite angles (α) in complexes **7**, **18**, and **19-TS**. (d) Computed buried volume (%V_{Bur}) of the bidentate phosphine ligands in complexes **7**, **18**, and **19-TS**.

insertion step with four different bidentate phosphine ligands, dppm, dppe, dppp, and dppb (Figure 8a).[34] Good agreement with the experimental reactivity trend was obtained. The experimentally most effective dppb ligand has a barrier of more than 3 kcal/mol lower than other ligands tested. In Figure 8a, we dissected the overall barrier into the energy difference between the resting state **7** and the intermediate **18** before the CO insertion, ΔG(**7**-**18**), and the energy of the CO insertion transition state **19-TS** with respect to **18**, $\Delta G^{\ddagger}$(**18**-**19-TS**). While bulkier ligands lead to a less stable six-coordinated intermediate **18** (ΔG(**7**-**18**) is 15.6, 16.6, 19.2, and 20.5 kcal/mol for dppm, dppe, dppp, and dppb, respectively), they dramatically decrease the carbonyl insertion barrier, $\Delta G^{\ddagger}$(**18**-**19-TS**), from 17.2 kcal/mol with dppm to 7.6 kcal/mol with dppb. The facile carbonyl insertion from intermediate **18** is clearly the major factor that contributes to the increased reactivity with bulkier ligand.

We next explored the correlation of the reactivity with two widely used parameters for ligand steric properties, bite angle (β) and buried volume (%V_{Bur}). The P−Rh−P bite angle is taken from various computed structures and compared with the average ligand bite angle in X-ray structures reported in the literature (Figure 8b).[19a] The buried volume (Figure 8d), defined as the percentage of volume occupied by the ligand in the first coordination sphere of the metal,[20,23] offers a different perspective, since it takes into account the steric bulk of the whole ligand. Here, the observed reactivity demonstrated better correlation with ligand bite angle than with buried volume. In particular, the computed buried volume values are similar for dppp and dppb, in line with previous reports of other metal complexes,[20] while dppb is predicted to be much more reactive than dppp. These results suggest the CO insertion reactivity is more sensitive to the steric environment in the P−Rh−P plane than to the overall steric bulk of the ligand. This is attributed to the nature of the rate-determining transition state **19-TS**, where the CO insertion occurs in the plane of the bisphosphine ligand. This CO insertion process accompanies a noticeable decrease of the substrate bite angle (α, defined as the Cl−Rh−C angle in **7** and the C−Rh−C angle in **18** and **19-TS**) from 85−90° to about 55° (Figure 8c).

Monitoring the changes in ligand bite angle and buried volume from **7** and **18** to **19-TS** allowed us to investigate the degree of distortion of the ligands and the amount of strain release during the reaction. The computed bite angles in **19-TS** are always the closest to the literature values, while the bite angles in **18** are smaller than in the corresponding transition states (Figure 8b). Similarly, the computed buried volumes in **18** are also significantly smaller than those in **19-TS** (Figure 8d). The smaller bite angle and buried volume in **18** indicate greater ligand distortion due to crowdedness around the metal center. The changes in bite angles and buried volumes are the greatest for dppb, suggesting greater amount of strain release during the CO insertion with the bulky ligand. In addition, the change of substrate bite angle α from **7** to **19-TS** with dppb is the smallest among all four ligands, indicating smaller amount of substrate distortion required in the CO insertion transition state.

To better illustrate the steric repulsions at different regions of the ligand and to monitor the change of ligand steric environment during the CO insertion, we plotted 2D steric contour maps of the van der Waals surface of the ligands.[21] The previously reported procedures to generate the steric contour maps were used and are illustrated in Scheme 5. The ligand

Scheme 5. Procedures to Generate the Ligand Steric Contours[a]

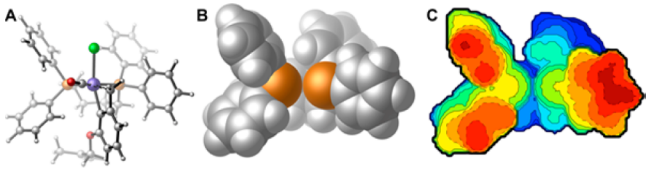

[a](A) Optimized geometry of a transition state; (B) van der Waals surface of the ligand; and (C) color-coded 2D steric contour map.

DOI: 10.1021/jacs.5b04691
J. Am. Chem. Soc. 2015, 137, 8274−8283

geometries are taken from the optimized structures of the intermediate **7** and transition state **19-TS** (Scheme 5A). The contours are generated from the van der Waals surface (Scheme 5B) of the ligand along the axis of the Rh atom and the midpoint between the two P atoms. The color on the contour map indicates the distance to the substrate; red indicates "blocked" areas where the atoms on the ligand are closest to the substrate, while blue indicates areas that are away from the substrate. The computed steric contours can provide more precise illustrations of the steric hindrance at different regions of the ligand than qualitative models such as the widely used quadrant diagrams for analysis of ligand–substrate interactions.[35]

The ligand steric contours of the resting state **7** and the rate-determining CO insertion transition state **19-TS** are shown in Figure 9. The majority of the steric bulk of the ligand (red and yellow areas) is attributed to the Ph groups located close to the P–Rh–P plane. As a result, steric clashing with the Cl atom and the CH_2 group attached to the Rh are expected in the resting state **7**. The contour maps revealed the distinct steric environment of the different ligands. The Ph groups on the dppb ligand are placed much closer to the substrate, while minimal substrate–ligand interactions are expected with the dppm and dppe ligands. In the CO insertion transition state **19-TS**, the ligand–substrate steric interaction is diminished as the substrate bite angle (α) decreases by more than 30°. The release of steric strain leads to the increase of the P–Rh–P angle (see discussion above), and the Ph groups are thus seen being closer to the substrate in **19-TS** (i.e., more red and yellow areas than in **7**). The greatest ligand conformational change from **7** to **19-TS** is observed with dppb, in line with the greater change of ligand bite angle with this ligand.

Origin of Enantioselectivity. When chiral ligands such as (*R*)-DTBM-SEGPHOS or (*R*)-SEGPHOS were employed, the Rh-catalyzed carboacylation leads to high level of enantioselectivity (Scheme 1b).[4b] The absolute configuration of the product was confirmed by X-ray crystallography. Here we calculated the enantioselectivity-determining olefin migratory insertion transition states using the computationally less demanding (*R*)-SEGPHOS ligand. In experiment, (*R*)-SEGPHOS yielded similarly high level of enantioselectivity (97% ee versus 98% ee with (*R*)-DTBM-DEGPHOS), albeit with lower yield.

The geometries and activation energies of the two transition states leading to the enantiomeric products are shown in Figure 10. The lower energy transition state **29-TS** leads to the major (*R*)-product observed in experiment, while **30-TS** leads to the (*S*)-product. The computed activation energy difference of 5.4 kcal/mol correlates well with the observed high level of enantioselectivity. The (*R*)-SEGPHOS ligand adopts the axial–equatorial conformation,[36] placing the two equatorial phenyl groups closer to the substrate. The origin of enantioselectivity arises from the steric repulsions between the SEGPHOS ligand and the C8 methylene group (highlighted in green) in the substrate. In both **29-TS** and **30-TS**, the methylene group (C8) is tilted toward the catalyst during the formation of the fused ring. This methylene group is placed in the empty quadrant of the Rh[(*R*)-SEGPHOS] complex in **29-TS**, while placed in a quadrant occupied by the highlighted equatorial phenyl group in **30-TS**. The steric repulsions between the methylene group and the ligand in **30-TS** are evidenced by the conformational change of the ligand from the resting state (**28**). The highlighted equatorial phenyl group on the ligand remains

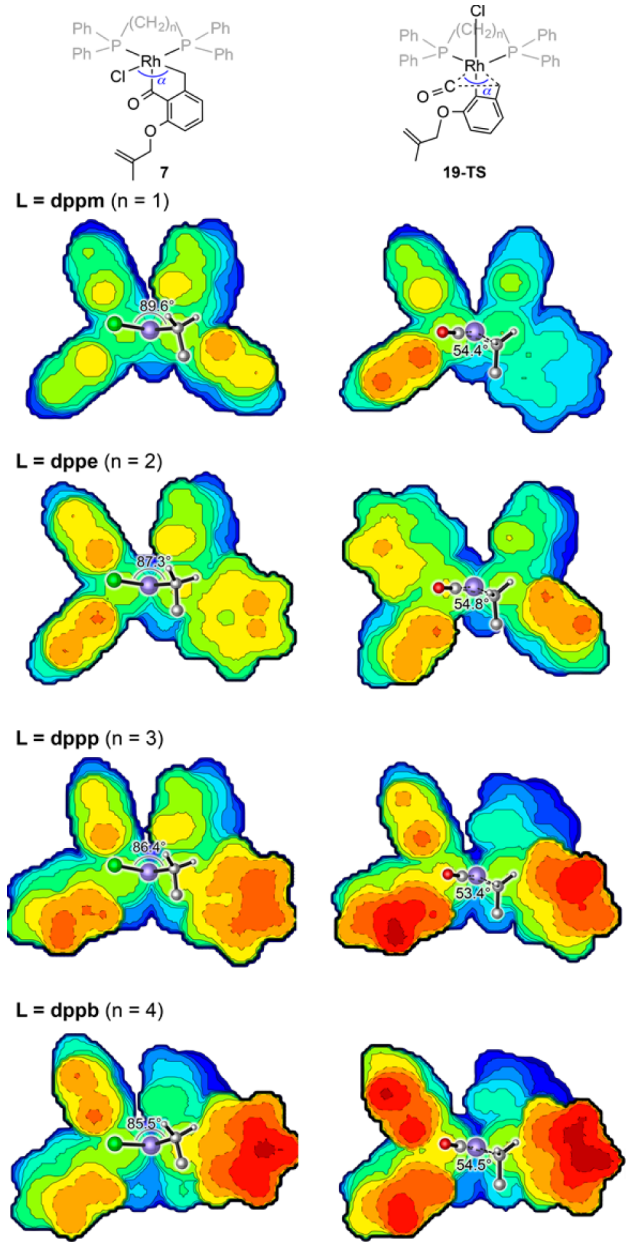

Figure 9. Steric contour maps of ligands dppm, dppe, dppp, and dppb in the catalyst resting state **7** and the rate-determining CO insertion transition state **19-TS**. The rhodium atom (purple), the Cl (green), CO (gray and red), and alkyl (gray) groups attached to the rhodium are shown to illustrate the substrate–ligand steric interactions.

the same conformation in **28** and **29-TS**, while the same phenyl group undergoes significant conformational change in **30-TS** compared to **28** due to the repulsions with the substrate (Figure 10). This conformation leads to steric clash between the C8 methylene on the substrate and one of the backbone aryl groups on the ligand. The difference of steric interactions in the transition states can be noted from the shorter ligand–substrate distance in **30-TS** than in **29-TS** (2.09 and 2.23 Å, respectively).

CONCLUSIONS

The mechanism, reactivity, regio-, and enantioselectivities in Rh-catalyzed carboacylation of benzocyclobutenones were investigated using DFT calculations. The benzocyclobutenone

DOI: 10.1021/jacs.5b04691
J. Am. Chem. Soc. 2015, 137, 8274–8283

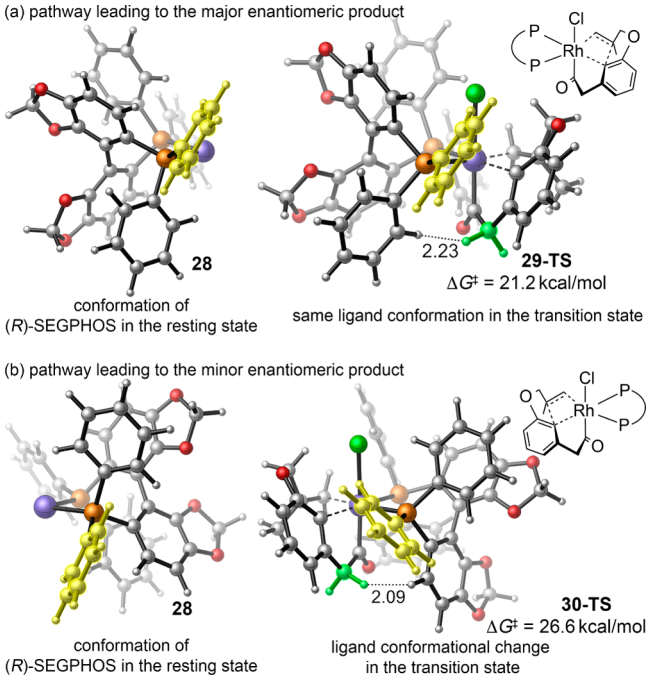

Figure 10. Olefin migratory insertion transition states with (*R*)-SEGPHOS ligand. The equatorial phenyl group (highlighted in yellow) of (*R*)-SEGPHOS occupies the top-front and bottom-front quadrant in **29-TS** and **30-TS**, respectively.

cleavage occurs via oxidative addition of the relatively weak C1−C8 bond[3] to form a benzorhodacyclopentenone intermediate. The regioisomeric pathway for the C1−C2 bond oxidative addition requires a higher barrier. Although the C1−C8 bond oxidative addition is irreversible, subsequent decarbonylation and CO insertion lead to the isomerization of the rhodacycle to form the more stable C1−C2 bond activation intermediate. After olefin migratory insertion and reductive elimination, the tricyclic ketone product is formed.

CO insertion, a key step in the rhodacycle isomerization to the C1−C2 bond activation intermediate, is rate-determining. This step is promoted by ligands with large bite angles, such as dppb. Analysis of ligand bite angle, buried volume, and ligand steric contour maps of a series of bisphophine ligands revealed that the increase of reactivity of bulky ligand is attributed to the release of ligand−substrate repulsions in the P−Rh−P plane during the CO insertion step. Thus, the reactivity correlates better with the ligand bite angle than with the overall steric bulk of the ligand. The intramolecular olefin migratory insertion occurs after the rhodacycle isomerization and is irreversible. Thus, this step determines the enantioselectivity in reactions with chiral ligands. Computed transition-state structures with the (*R*)-SEGPHOS ligand indicated the observed enantioselectivity is attributed to the steric repulsion between the C8 methylene group in the substrate and the equatorial phenyl group of the chiral ligand.

■ ASSOCIATED CONTENT

Supporting Information

Structures and energies of all isomers of intermediates and transition states, Cartesian coordinates of all computed structures. The Supporting Information is available free of charge on the ACS Publications website at DOI: 10.1021/jacs.5b04691.

■ AUTHOR INFORMATION

Corresponding Author

*pengliu@pitt.edu

Notes

The authors declare no competing financial interest.

■ ACKNOWLEDGMENTS

We thank the University of Pittsburgh (P.L.), NIGMS (R01GM109054-01, G.D.) and the Welch Foundation (F 1781, G.D.) for funding. Yang Yang (Buchwald group, MIT) is acknowledged for helpful discussions. Calculations were performed at the Center for Simulation and Modeling at the University of Pittsburgh and the Extreme Science and Engineering Discovery Environment (XSEDE) supported by NSF.

■ REFERENCES

(1) For reviews on C−C bond activation: (a) Murakami, M.; Ito, Y. *Top. Organomet. Chem.* **1999**, *3*, 97−129. (b) Jun, C.-H. *Chem. Soc. Rev.* **2004**, *33*, 610−618. (c) Satoh, T.; Miura, M. *Top. Organomet. Chem.* **2005**, *14*, 1−20. (d) Jun, C.-H.; Park, J.-W. *Top. Organomet. Chem.* **2007**, *24*, 117−143. (e) Necas, D.; Kotora, M. *Curr. Org. Chem.* **2007**, *11*, 1566−1591. (f) Park, Y.-J.; Park, J.-W.; Jun, C.-H. *Acc. Chem. Res.* **2008**, *41*, 222−234. (g) Seiser, T.; Cramer, N. *Org. Biomol. Chem.* **2009**, *7*, 2835−2840. (h) Winter, C.; Krause, N. *Angew. Chem., Int. Ed.* **2009**, *48*, 2460−2462. (i) Murakami, M.; Matsuda, T. *Chem. Commun.* **2011**, *47*, 1100−1105. (j) Dong, G. *Synlett* **2013**, *24*, 1−5. (k) Jiao, L.; Yu, Z.-X. *J. Org. Chem.* **2013**, *78*, 6842−6848. (l) Liu, H.; Feng, M.; Jiang, X. *Chem.-Asian J.* **2014**, *9*, 3360−3389. (m) Chen, F.; Wang, T.; Jiao, N. *Chem. Rev.* **2014**, *114*, 8613−8661. (n) Dermenci, A.; Coe, J. W.; Dong, G. *Org. Chem. Front.* **2014**, *1*, 567−584. (o) C−C bond activation. In *Topics in Current Chemistry*; Dong, G., Ed.; Springer-Verlag: Berlin, 2014; Vol. *346*. (p) Souillart, L.; Cramer, N. *Chem. Rev.*, **2015**, ASAP, DOI: 10.1021/acs.chemrev.5b00138.

(2) (a) Bellus, D.; Ernst, B. *Angew. Chem., Int. Ed. Engl.* **1988**, *27*, 797−827. (b) Cramer, N.; Seiser, T. *Synlett* **2011**, 449−460. (c) Seiser, T.; Saget, T.; Tran, D. N.; Cramer, N. *Angew. Chem., Int. Ed.* **2011**, *50*, 7740−7752. (d) Xia, Y.; Liu, Z.; Liu, Z.; Ge, R.; Ye, F.; Hossain, M.; Zhang, Y.; Wang, J. *J. Am. Chem. Soc.* **2015**, *136*, 3013−3015. (e) Marek, I.; Masarwa, A.; Delaye, P.-O.; Leibeling, M. *Angew. Chem., Int. Ed.* **2015**, *54*, 414−429. (f) Fu, X.-F.; Xiang, Y.; Yu, Z.-X. *Chem.−Eur. J.* **2015**, *21*, 4242−4246.

(3) Cleavage of the C1−C8 bond in benzocyclobutenone **1** to form vinyl ketene **12** is endergonic by 19.3 kcal/mol (Figure 3). This process is much more favorable thermodynamically than the cleavage of the C1−C2 bond, which requires 72.2 kcal/mol.

(4) (a) Xu, T.; Dong, G. *Angew. Chem., Int. Ed.* **2012**, *51*, 7567−7571. (b) Xu, T.; Ko, H. M.; Savage, N. A.; Dong, G. *J. Am. Chem. Soc.* **2012**, *134*, 20005−20008. (c) Xu, T.; Dong, G. *Angew. Chem., Int. Ed.* **2014**, *53*, 10733−10736.

(5) Xu, T.; Savage, N. A.; Dong, G. *Angew. Chem., Int. Ed.* **2014**, *53*, 1891−1895.

(6) Chen, P.; Xu, T.; Dong, G. *Angew. Chem., Int. Ed.* **2014**, *53*, 1674−1678.

(7) For experimental mechanistic studies of Rh-catalyzed intramolecular carboacylation of quinolinyl ketones with tethered alkenes: (a) Rathbun, C. M.; Johnson, J. B. *J. Am. Chem. Soc.* **2011**, *133*, 2031−2033. (b) Lutz, J. P.; Rathbun, C. M.; Stevenson, S. M.; Powell, B. M.; Boman, T. S.; Baxter, C. E.; Zona, J. M.; Johnson, J. B. *J. Am. Chem. Soc.* **2012**, *134*, 715−722. For the original experimental report on this reaction: (c) Dreis, A. M.; Douglas, C. J. *J. Am. Chem. Soc.* **2009**, *131*, 412−413.

(8) (a) Aissa, C. *Synthesis-Stuttgart* **2011**, 3389−3407. (b) Ruhland, K. *Eur. J. Org. Chem.* **2012**, 2683−2706.

(9) Computational studies on C−CN bond activation with Ni: (a) Atesin, T. A.; Li, T.; Lachaize, S.; Garcia, J. J.; Jones, W. D. *Organometallics* **2008**, *27*, 3811−3817. (b) Li, T.; Garcia, J. J.;

DOI: 10.1021/jacs.5b04691
J. Am. Chem. Soc. 2015, 137, 8274−8283

Brennessel, W. W.; Jones, W. D. *Organometallics* **2010**, *29*, 2430−2445. (c) Evans, M. E.; Li, T.; Jones, W. D. *J. Am. Chem. Soc.* **2010**, *132*, 16278−16284. (d) Li, T.; Jones, W. D. *Organometallics* **2011**, *30*, 547−555. (e) Guan, W.; Sakaki, S.; Kurahashi, T.; Matsubara, S. *ACS Catal.* **2015**, *5*, 1−10. Pt: (f) Miscione, G. P.; Bottoni, A. *Organometallics* **2014**, *33*, 4173−4182. Rh: (g) Jiang, Y.-Y.; Yu, H.-Z.; Fu, Y. *Organometallics* **2013**, *32*, 926−936. (h) Zhang, S.-L.; Huang, L.; Bie, W.-F. *Organometallic* **2014**, *33*, 3030−3039.

(10) (a) Yu, Z. X.; Wender, P. A.; Houk, K. N. *J. Am. Chem. Soc.* **2004**, *126*, 9154−9155. (b) Yu, Z.-X.; Cheong, P. H.-Y.; Liu, P.; Legault, C. Y.; Wender, P. A.; Houk, K. N. *J. Am. Chem. Soc.* **2008**, *130*, 2378−2379. (c) Liu, P.; Cheong, P. H.-Y.; Yu, Z.-X.; Wender, P. A.; Houk, K. N. *Angew. Chem., Int. Ed.* **2008**, *47*, 3939−3941. (d) Liu, P.; Sirois, L. E.; Cheong, P. H.-Y.; Yu, Z.-X.; Hartung, I. V.; Rieck, H.; Wender, P. A.; Houk, K. N. *J. Am. Chem. Soc.* **2010**, *132*, 10127−10135. (e) Jiao, L.; Lin, M.; Yu, Z.-X. *J. Am. Chem. Soc.* **2011**, *133*, 447−461. (f) Xu, X.; Liu, P.; Lesser, A.; Sirois, L. E.; Wender, P. A.; Houk, K. N. *J. Am. Chem. Soc.* **2012**, *134*, 11012−11025. (g) Ganesh, V.; Sureshkumar, D.; Chanda, D.; Chandrasekaran, S. *Chem.—Eur. J.* **2012**, *18*, 12498−12511. (h) Hong, X.; Stevens, M. C.; Liu, P.; Wender, P. A.; Houk, K. N. *J. Am. Chem. Soc.* **2014**, *136*, 17273−17283. (i) Orr, D.; Percy, J. M.; Tuttle, T.; Kennedy, A. R.; Harrsion, Z. A. *Chem.—Eur. J.* **2014**, *20*, 14305−14316.

(11) Pd-catalyzed cyclopropylidene (3 + 2) cycloaddition: (a) García-Fandiño, R.; Gulías, M.; Castedo, L.; Granja, J. R.; Mascareñas, J. L.; Cárdenas, D. J. *Chem.—Eur. J.* **2008**, *14*, 272−281. (b) García-Fandiño, R.; Gulías, M.; Mascareñas, J. L.; Cárdenas, D. J. *Dalton Trans.* **2012**, *41*, 9468−9481. Ni-catalyzed cyclopropylidene (3 + 2) cycloaddition: (c) An, Y.; Cheng, C.; Pan, B.; Wang, Z. *Eur. J. Org. Chem.* **2012**, *21*, 3911−3915. (d) Komagawa, S.; Wang, C.; Morokuma, K.; Saito, S.; Uchiyama, M. *J. Am. Chem. Soc.* **2013**, *135*, 14508−14511.

(12) Werz, D. B.; Klatt, G.; Raskatov, J. A.; Koeppel, H.; Gleiter, R. *Organometallics* **2009**, *28*, 1675−1682.

(13) For computational studies on C−C bond activation with other substrates. Cyclopentadiene: (a) Khoroshun, D. V.; Inagaki, A.; Suzuki, H.; Vyboishchikov, S. F.; Musaev, D. G.; Morokuma, K. *J. Am. Chem. Soc.* **2003**, *125*, 9910−9911. Biphenylene: (b) Chaplin, A. B.; Tonner, R.; Weller, A. S. *Organometallics* **2010**, *29*, 2710−2714. (c) Darmon, J. M.; Stieber, S. C. E.; Sylvester, K. T.; Fernandez, I.; Lobkovsky, E.; Semproni, S. P.; Bill, E.; Wieghardt, K.; DeBeer, S.; Chirik, P. J. *J. Am. Chem. Soc.* **2012**, *134*, 17125−17137. 3-Azetidinone: (d) Li, Y.; Lin, Z. *Organometallics* **2013**, *32*, 3003−3011. Decarboxylation of aryl carboxylic acids: (e) Zhang, S.-L.; Fu, Y.; Shang, R.; Guo, Q.-X.; Liu, L. *J. Am. Chem. Soc.* **2010**, *132*, 638−646. (f) Xue, L.; Su, W.; Lin, Z. *Dalton Trans.* **2010**, *39*, 9815−9822.

(14) For computational studies on chelation-assisted metal-mediated stoichiometric aryl−acyl/alkyl bond cleavage: (a) Obenhuber, A.; Ruhland, K. *Organometallics* **2011**, *30*, 4039−4051. (b) Rybtchinski, B.; Oevers, S.; Montag, M.; Vigalok, A.; Rozenberg, H.; Martin, J. M. L.; Milstein, D. *J. Am. Chem. Soc.* **2001**, *123*, 9064−9077. (c) Montag, M.; Efremenko, I.; Diskin-Posner, Y.; Ben-David, Y.; Martin, J. M. L.; Milstein, D. *Organometallics* **2012**, *31*, 505−512.

(15) (a) Ding, L.; Ishida, N.; Murakami, M.; Morokuma, K. *J. Am. Chem. Soc.* **2014**, *136*, 169−178. (b) Yu, H.; Wang, C.; Yang, Y.; Dang, Z.-M. *Chem.—Eur. J.* **2014**, *20*, 3839−3848. (c) Masarwa, A.; Weber, M.; Sarpong, R. *J. Am. Chem. Soc.* **2015**, *137*, 6327−6334.

(16) (a) Huffman, M. A.; Liebeskind, L. S. *Organometallics* **1992**, *11*, 255−266. (b) Huffman, M. A.; Liebeskind, L. S. *Organometallics* **1990**, *9*, 2194−2196.

(17) For thermal electrocyclic ring-opening of cyclobutenones and benzocyclobutenones, see: (a) Danheiser, R. L.; Gee, S. K. *J. Org. Chem.* **1984**, *49*, 1672−1674. (b) Schiess, P.; Eberle, M.; Huysfrancotte, M.; Wirz, J. *Tetrahedron Lett.* **1984**, *25*, 2201−2204. (c) Danheiser, R. L.; Nishida, A.; Savariar, S.; Trova, M. P. *Tetrahedron Lett.* **1988**, *29*, 4917−4920.

(18) Previous experimental studies indicated the regioselectivity in metal-mediated cleavage of benzocyclobutenone is affected by the metal catalyst, ligand, substituents, and reaction conditions: (a) Huffman, M. A.; Liebeskind, L. S.; Pennington, W. T. *Organometallics* **1990**, *9*, 2194−2196. (b) Huffman, M. A.; Liebeskind, L. S.; Pennington, W. T. *Organometallics* **1992**, *11*, 255−266. (c) Joost, M.; Estévez, L.; Miqueu, K.; Amgoune, A.; Bourissou, D. *Angew. Chem., Int. Ed.* **2015**, *54*, 5236−5240.

(19) (a) Dierkes, P.; van Leeuwen, P. *J. Chem. Soc., Dalton Trans.* **1999**, 1519−1529. (b) van Leeuwen, P.; Kamer, P. C. J.; Reek, J. N. H.; Dierkes, P. *Chem. Rev.* **2000**, *100*, 2741−2769. (c) Kamer, P. C. J.; van Leeuwen, P. W. N.; Reek, J. N. H. *Acc. Chem. Res.* **2001**, *34*, 895−904. (d) Ledford, J.; Shultz, C. S.; Gates, D. P.; White, P. S.; DeSimone, J. M.; Brookhart, M. *Organometallics* **2001**, *20*, 5266−5276. (e) Daniels, D. S. B.; Jones, A. S.; Thompson, A. L.; Paton, R. S.; Anderson, E. A. *Angew. Chem., Int. Ed.* **2014**, *53*, 1915−1920.

(20) Clavier, H.; Nolan, S. P. *Chem. Commun.* **2010**, *46*, 841−861.

(21) (a) Ragone, F.; Poater, A.; Cavallo, L. *J. Am. Chem. Soc.* **2010**, *132*, 4249−4258. (b) Poater, A.; Ragone, F.; Mariz, R.; Dorta, R.; Cavallo, L. *Chem.—Eur. J.* **2010**, *16*, 14348−14353. (c) Liu, P.; Montgomery, J.; Houk, K. N. *J. Am. Chem. Soc.* **2011**, *133*, 6956−6959. (d) Wucher, P.; Caporaso, L.; Roesle, P.; Ragone, F.; Cavallo, L.; Mecking, S.; Gottker-Schnetmann, I. *Proc. Natl. Acad. Sci. U.S.A.* **2011**, *108*, 8955−8959.

(22) Frisch, M. J.; Trucks, G. W.; Schlegel, H. B.; Scuseria, G. E.; Robb, M. A.; Cheeseman, J. R.; Scalmani, G.; Barone, V.; Mennucci, B.; Petersson, G. A.; Nakatsuji, H.; Caricato, M.; Li, X.; Hratchian, H. P.; Izmaylov, A. F.; Bloino, J.; Zheng, G.; Sonnenberg, J. L.; Hada, M.; Ehara, M.; Toyota, K.; Fukuda, R.; Hasegawa, J.; Ishida, M.; Nakajima, T.; Honda, Y.; Kitao, O.; Nakai, H.; Vreven, T.; Montgomery, J. A., Jr.; Peralta, J. E.; Ogliaro, F.; Bearpark, M.; Heyd, J. J.; Brothers, E.; Kudin, K. N.; Staroverov, V. N.; Kobayashi, R.; Normand, J.; Raghavachari, K.; Rendell, A.; Burant, J. C.; Iyengar, S. S.; Tomasi, J.; Cossi, M.; Rega, N.; Millam, N. J.; Klene, M.; Knox, J. E.; Cross, J. B.; Bakken, V.; Adamo, C.; Jaramillo, J.; Gomperts, R.; Stratmann, R. E.; Yazyev, O.; Austin, A. J.; Cammi, R.; Pomelli, C.; Ochterski, J. W.; Martin, R. L.; Morokuma, K.; Zakrzewski, V. G.; Voth, G. A.; Salvador, P.; Dannenberg, J. J.; Dapprich, S.; Daniels, A. D.; Farkas, Ö.; Foresman, J. B.; Ortiz, J. V.; Cioslowski, J.; Fox, D. J. *Gaussian 09*, Revision D.01; Gaussian, Inc.: Wallingford, CT, 2009.

(23) Poater, A.; Cosenza, B.; Correa, A.; Giudice, S.; Ragone, F.; Scarano, V.; Cavallo, L. *Eur. J. Inorg. Chem.* **2009**, 1759−1766.

(24) (a) Tanaka, K.; Shibata, Y.; Suda, T.; Hagiwara, Y.; Hirano, M. *Org. Lett.* **2007**, *9*, 1215−1218. (b) Murphy, S. K.; Bruch, A.; Dong, V. M. *Angew. Chem., Int. Ed.* **2014**, *53*, 2455−2459. (c) Murphy, S. K.; Bruch, A.; Dong, V. M. *Chem. Sci.* **2015**, *6*, 174−180.

(25) (a) Tobisu, M.; Hyodo, I.; Onoe, M.; Chatani, N. *Chem. Commun.* **2008**, 6013−6015. (b) Gandeepan, P.; Cheng, C.-H. *J. Am. Chem. Soc.* **2012**, *134*, 5738−5741. (c) Yang, Y.; Buchwald, S. L. *Angew. Chem., Int. Ed.* **2014**, *53*, 8677−8681. (d) Yang, Y.; Liu, P. *ACS Catal.* **2015**, *5*, 2944−2951.

(26) (a) Johnson, J. B.; Rovis, T. *Angew. Chem., Int. Ed.* **2008**, *47*, 840−871. (b) Miller, K. M.; Luanphaisarnnont, T.; Molinaro, C.; Jamison, T. F. *J. Am. Chem. Soc.* **2004**, *126*, 4130−4131. (c) Jang, H.-Y.; Huddleston, R. R.; Krische, M. J. *J. Am. Chem. Soc.* **2004**, *126*, 4664−4668. (d) Liu, P.; McCarren, P.; Cheong, P. H.-Y.; Jamison, T. F.; Houk, K. N. *J. Am. Chem. Soc.* **2010**, *132*, 2050−2057.

(27) The geometry optimization of **9-TS** was performed with M06/LANL2DZ-6-31G(d). Geometry optimization using B3LYP failed to locate the olefin-bound transition state **9-TS**. The single-point energy calculation of **9-TS** was performed at the same level (M06/SDD-6-311+G(d,p)/SMD(toluene)) as other structures.

(28) (a) Matsuo, J.; Sasaki, S.; Tanaka, H.; Ishibashi, H. *J. Am. Chem. Soc.* **2008**, *130*, 11600−11601. (b) Robinson, J. M.; Tlais, S. F.; Fong, J.; Danheiser, R. L. *Tetrahedron* **2011**, *67*, 9890−9898. (c) Souillart, L.; Cramer, N. *Chem.—Eur. J.* **2015**, *21*, 1863−1867.

(29) Niwayama, S.; Kallel, E. A.; Sheu, C.; Houk, K. N. *J. Org. Chem.* **1996**, *61*, 2517−2522.

(30) For examples of catalytic decarbonylations of ketones: (a) Murakami, M.; Amii, H.; Ito, Y. *Nature* **1994**, *370*, 540−541. (b) Murakami, M.; Amii, H.; Shigeto, K.; Ito, Y. *J. Am. Chem. Soc.* **1996**, *118*, 8285−8290. (c) Daugulis, O.; Brookhart, M. *Organo-*

DOI: 10.1021/jacs.5b04691
J. Am. Chem. Soc. 2015, 137, 8274−8283

metallics **2004**, *23*, 527−534. (d) Matsuda, T.; Shigeno, M.; Murakami, M. *Chem. Lett.* **2006**, *35*, 288−289. (e) Lei, Z.-Q.; Li, H.; Li, Y.; Zhang, X.-S.; Chen, K.; Wang, X.; Sun, J.; Shi, Z.-J. *Angew. Chem., Int. Ed.* **2012**, *51*, 2690−2694. (f) Dermenci, A.; Whittaker, R. E.; Dong, G. *Org. Lett.* **2013**, *15*, 2242−2245. (g) Dermenci, A.; Whittaker, R. E.; Gao, Y.; Cruz, F. A.; Yu, Z.-X.; Dong, G. *Chem. Sci.* **2015**, *6*, 3201−3210. For a recent review, see: (h) Dermenci, A.; Dong, G. *Sci. China Chem.* **2013**, *56*, 685−701.

(31) For recent reviews of catalytic CO insertions: (a) Franke, R.; Selent, D.; Boerner, A. *Chem. Rev.* **2012**, *112*, 5675−5732. (b) Beller, M.; Wu, X. -F. *Transition Metal Catalyzed Carbonylation Reactions: Carbonylative Activation of C-X Bonds*; Springer: Amsterdam, 2013. (c) Pospech, J.; Fleischer, I.; Franke, R.; Buchholz, S.; Beller, M. *Angew. Chem., Int. Ed.* **2013**, *52*, 2852−2872. (d) Wu, X.-F.; Fang, X.; Wu, L.; Jackstell, R.; Neumann, H.; Beller, M. *Acc. Chem. Res.* **2014**, *47*, 1041−1053.

(32) Murakami, M.; Itahashi, T.; Amii, H.; Takahashi, K.; Ito, Y. *J. Am. Chem. Soc.* **1998**, *120*, 9949−9950.

(33) The computed barrier of the alkene migratory insertion step in the reaction with substrate **1a** is 27.3 kcal/mol. The experimentally used solvent THF was used in the solvation energy calculation for this reaction.

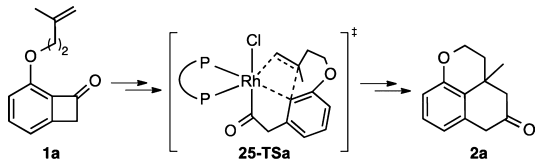

(34) With all four ligands, the decarbonylation/CO insertion mechanism is found to be more favorable than the alternative rhodacycle isomerization pathway involving reversible oxidative addition (**7** → **6-TS** → **3** → **4-TS** → **5**), although the difference in activation energies becomes smaller with the less reactive dppm and dppe ligands. See the Supporting Information for details.

(35) Knowles, W. S. *Angew. Chem., Int. Ed.* **2002**, *41*, 1998−2007.

(36) Jeulin, S.; Duprat de Paule, S.; Ratovelomanana-Vidal, V.; Genêt, J.-P.; Champion, N.; Dellis, P. *Proc. Natl. Acad. Sci. U.S.A.* **2004**, *101*, 5799−5804.

DOI: 10.1021/jacs.5b04691
J. Am. Chem. Soc. 2015, 137, 8274−8283